Journal of Magnetism and Magnetic Materials 361 (2014) 118–125

Contents lists available at ScienceDirect

Journal of Magnetism and Magnetic Materials

journal homepage: www.elsevier.com/locate/jmmm

Comparison of different methodologies for obtaining nickel nanoferrites

R. Galindo [a], N. Menendez [a], P. Crespo [b], V. Velasco [b], O. Bomati-Miguel [c], D. Díaz-Fernández [c], P. Herrasti [a,*]

[a] Departamento de Química Física Aplicada, Facultad de Ciencias, Universidad Autónoma de Madrid, Cantoblanco, E-28049 Madrid, Spain
[b] Instituto de Magnetismo Aplicado, UCM, ADIF CSIC, E-28230 Madrid, Spain
[c] Departamento de Física Aplicada and Instituto Nicolás Cabrera, Facultad de Ciencias Universidad Autónoma de Madrid, Cantoblanco, E-28049 Madrid, Spain

ARTICLE INFO

Article history:
Received 5 September 2013
Received in revised form
13 January 2014
Available online 3 March 2014

Keywords:
Coprecipitation
Electrochemistry
Nickel ferrite
Sonochemistry
Sonoelectrochemistry

ABSTRACT

Nickel nanoferrites were obtained by means of four different synthetic wet-routes: co-precipitation (CP), sonochemistry (SC), sonoelectrochemistry (SE) and electrochemistry (E). The influence of the synthesis method on the structural and magnetic properties of nickel ferrite nanoparticles is studied. Although similar experimental conditions such as temperature, pH and time of synthesis were used, a strong dependence of composition and microstructure on the synthesis procedure is found, as electron microscopy, X-ray diffraction and Mössbauer spectroscopy studies reveal. Whereas by means of the CP and SC methods particles of a small size around 5–10 nm, respectively, and composed by different phases are obtained, the electrochemical routes (E and SE) allow obtaining monodisperse nanoparticles, with sizes ranging from 30 to 40 nm, and very close to stoichiometry. Magnetic characterization evidences a superparamagnetic behavior for samples obtained by CP and SC methods, whereas the electrochemical route leads to ferromagnetic ferrite nanoparticles.

1. Introduction

In the last decades, nanomaterials have been widely studied due to their unique properties, from the beginning of the promising nanoscience, forecasted by Richard Feynman in 1959, until the much modern uses of nanotechnology [1–3]. Nanomaterial science opens up an infinite field of research and practical applications. In this sense millions of dollars are being invested in the study and development of new nanomaterials with attractive potential applications. This enthusiasm for nanoparticles has been spread out to the field of the magnetic nanoparticles.

Magnetic nanoparticles (MNPs) have been intensely investigated in recent years, mainly on account of their attractive and unique physical and chemical properties, such as huge specific surface area, good electrocatalytic activity and low cost, among others. Moreover, MNPs are a class of materials that could be manipulated under the influence of an external magnetic field [4–8]. Magnetic nanoparticles have been recently investigated for solving various environmental problems, such as removing toxic metal ions and radioactive elements, capturing of microbial pathogens and organic dyes, accelerating the coagulation of sewage, and remediation of contaminants. Magnetic nanoparticles can be reused after magnetic separation by removing the adsorbed toxic compounds [16]. Recent studies sought to adsorb heavy metals as Cr (VI) onto magnetic nanoparticles compared favorably with other adsorbents like activated carbon clay. The results have shown that magnetic nanostructured particles can be successfully applied to adsorb metal ions, in which the combined technique of bioabsorption and magnetic separations holds the advantages of flexibility, eco-friendly characteristics and economic in operational cost [17,18]

In particular, ferrites are one of the most widely used magnetic nanoparticles, and nickel ferrite, $NiFe_2O_4$, is one of the most important. Ferrites have been used as catalysts for some industrial important reactions such as hydrocarbons oxidation [9], dehydration and alcohols dehydrogenation [10,11], alkylation reactions [12] and glucose electroxidation [13]. The catalytic effectiveness of these systems arises from the ability of the metallic ions to migrate between the sublattices without altering the structure, which makes the catalyst suitable and efficient for many organic transformation reactions [14]. The catalytic activity of ferrites depends on their stability, particle size and distribution [15].

An accurate control of size and shape is one of the principal issues to be improved by the synthesis route. Monodisperse

* Corresponding author. Tel.: +34 914974831.
E-mail address: pilar.herrasti@uam.es (P. Herrasti).

http://dx.doi.org/10.1016/j.jmmm.2014.02.091
0304-8853

$NiFe_2O_4$ nanocrystals have been prepared by thermolysis or by the hydrolysis method. Liu et al. [19] have synthesized $NiFe_2O_4$ nanoparticles by the shock waves method. Superparamagnetic nickel ferrites NPs with diameters less than 10 nm have been produced by methods like sonochemical decomposition process, reverse micelle and aging treatment of the precipitated precursor at 145 °C [20]. The sol–gel method and reverse microemulsion processes have been also employed to prepare aggregate $NiFe_2O_4$ particles at room temperature [21]. Other used methods are solid state reaction, solvothermal, mechanosynthesis, hydrothermal [22,23], combustion techniques [24], and co-precipitation [25,26].

Each of the aforementioned synthesis processes has advantages and disadvantages, the most common disadvantage being the simultaneous synthesis of undesired compounds such as hydroxides, the dispersion in size of the obtained nanoparticles and the low yield of the process.

In this work a systematic study of nickel ferrites properties obtained under the same synthesis conditions without any further post-treatment using four methods is reported. It will be shown that electrochemical routes allow the synthesis of almost stoichiometric Ni ferrites whereas by the chemical procedures, coprecipitation and sonochemistry, the obtained nanoparticles show a mixture of different compounds.

2. Experimental

2.1. Synthesis of nanoparticles

2.1.1. Coprecipitation method (CO)

Coprecipitation is one of the most common and widely-used techniques for the production of nickel ferrites in particular and nanoparticles in general. In our work, the synthesis involved the preparation of 150 mL of a 2 M solution of NaOH (97% Sigma-Aldrich), kept constantly at 60 °C via a thermostat throughout the synthesis process, together with vigorous magnetic stirring. Once the required temperature was reached, 25 mL of a 0.1 M solution of $FeCl_3$ (Technical) and 25 mL of a 0.05 M solution of $NiCl_2$ (Technical) were added. The reaction was kept under the same conditions of stirring and temperature for 30 min. The end product was then repeatedly rinsed with distilled water and the precipitate recovered by successive centrifugation at 8000 rpm for 15 min. Finally, it was left to dry in a vacuum for a period of 12 h at 60 °C.

2.2. Sonochemical method (SC)

The solution used was the same as that indicated in the previous case, although in this case ultrasonic waves were applied instead of magnetic stirring. The frequency of the sonicator was 1040 kHz.

2.3. Electrochemical method (E)

The electrochemical method can be considered as a co-precipitation method with a control of the ions in solution by means of the current applied. The method consists in applying currents to two sheets of iron (Goodfellow 99.5%) and nickel (Goodfellow 99%) each with a 1 cm^2 electroactive area and placed 1 cm apart. These electrodes are surrounded by an iron sheet with a 67 cm^2 electroactive area as the cathode. The electrodes were then immersed in a 0.04 M tetramethyl ammonium chloride $(CH_3)_4NCl$ (Merck) as electrolyte. A 100 mA current was applied to the iron anode and a 50 mA current to the nickel anode to achieve a ratio of 2:1 between the iron and the nickel in the end product. To close the circuit, 150 mA were applied to the cathode. Synthesis was also kept at 60 °C under vigorous magnetic stirring for 30 min. After this time, the nanoparticles obtained were rinsed and dried as in the previous cases.

2.4. Sonoelectrochemical method (SE)

The methodology to synthesize the ferrite nickel nanoparticles using this method is similar to that above mentioned for the electrochemical method with the variation of replacing the magnetic stirring by the application of ultrasonic waves at a frequency of 1040 kHz to the solution during synthesis.

In this work, the temperature was kept constant at 60° C in all synthesis procedures

3. Characterization of the nanoparticles

The crystalline structure of the synthesized nanomaterials was studied by X-ray diffraction (XRD) by using a Siemens D-5000 Diffractometer with CuKα radiation ($\lambda = 1.5418$ Å), fitted with a Bruker SOL-X detector (Si(Li)) energy dispersive detector suitable for samples presenting fluorescence.

The analysis of the Fe and Ni contents in the sample was done by using a Perkin-Elmer coupled plasma emission spectrophotometer, Optima model 2100 DV system, with a CNHS PERKIN ELMER 2400 element analyzer.

In order to determine the size and dispersion of the nanoparticles, transmission electron microscopy (TEM) measurements were taken in a Philips 200 kV Thecnai 20 Transmission Electron Microscope.

Mössbauer measurements were performed in triangular mode at room temperature on a conventional spectrometer with a ^{57}Co (Rh) source. The spectra were analyzed with a non-linear fit using the NORMOS program [27].

X-ray photoelectron spectroscopy (XPS) was used for determining the surface composition. The spectra were measured in a CLAM-4 MCD spectrophotometer with a hemispherical analyzer system (Thermo VGScientific, 9-channeltron system) and a double anode source (model number XR3E2) with Al Kα and Mg Kα radiations in a UHV chamber (under 3×10^{-10} mbar of pressure).

The magnetization characterization was carried out with a Quantum Design SQUID magnetometer, MPMS model. Hysteresis loops as a function of the temperature have been measured between 5 and 300 K. The thermal dependence of the magnetization after cooling the samples under zero field conditions as well as under an applied field of 100 Oe has been measured for all samples.

4. Results and discussion

Fig. 1 shows the diffractograms for the nickel ferrite samples synthesized by (a) co-precipitation (CP), (b) sonochemistry (SC), (c) electrochemistry (E) and (d) sonoelectrochemistry (SE).

The diffractograms for the samples using methods CP and SC (Fig. 1a and b) exhibit broad peaks while the diffractograms of samples obtained using methods E and SE, (Fig. 1c and d) present narrow peaks. Since peak width is correlated to crystal size, very broad peaks should correspond to the samples having a very small crystal size. Moreover, the presence of multiple phases in the material may also lead to an apparent broadening of the diffraction peaks as a consequence of the overlapping of several peaks. In our case, both factors combine in these samples. Broad peaks can be indexed as corresponding to nickel ferrite, ferrihydrites and iron oxyhydroxides [28], thus demonstrating the presence of a mixture of compounds. Indexation of the pattern of the sample obtained by SC (Fig. 1c) reveals the presence of peaks characteristic

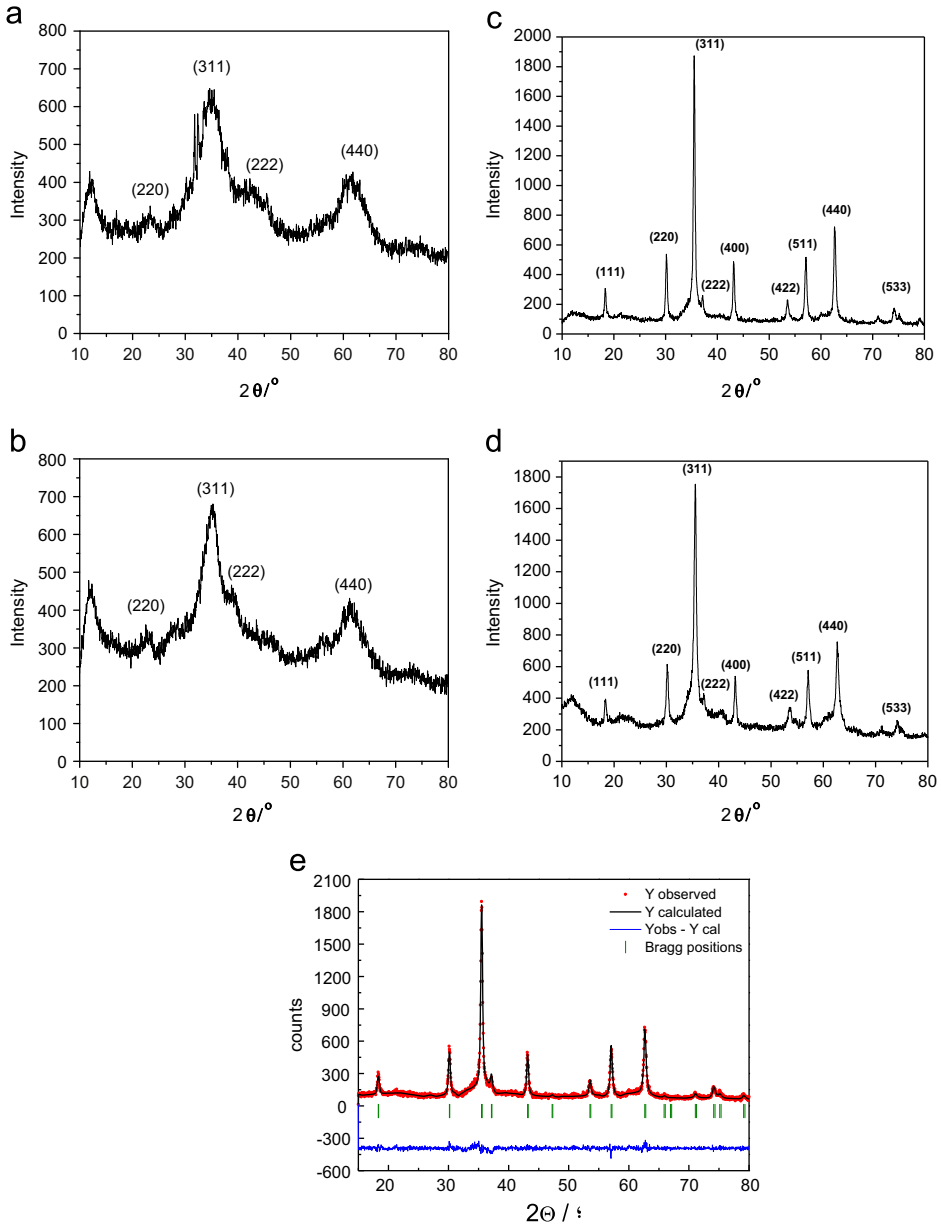

Fig. 1. XRD patterns of the nickel ferrite samples synthesized by (a) coprecipitation, (b) sonochemistry, (c) electrochemistry and (d) sonoelectrochemistry method. (e) X-ray diffractogram of electrochemical sample with the results of fitting by the Rietveld method.

of nickel ferrite, with the exception of one peak around $2\theta = 40^\circ$ that has been indexed as the plane (1 4 0) of an iron oxyhydroxide (FeOOH) (JCPDS 81-0453) [28]. Finally, in the diffractogram for the sample obtained using electrochemical method (Fig. 1d) only peaks corresponding to nickel ferrite are resolved, although the presence of Fe_3O_4 or γ-Fe_2O_3 cannot be a priorily discarded. The diffraction patterns of these compounds are very similar to the nickel ferrite [29].

Due to the co-existence of numerous phases in the samples obtained by CP and SC methods, it has not been possible to determine the crystallite size; for the nanoparticles obtained using E and SE methods the crystallite size is estimated, from the Scherrer's formula, to be 40 ± 10 and 29 ± 8 nm respectively.

In all the previously described methods, the process of nanoparticle formation occurs in an aqueous phase. This process takes place in two steps, nucleation and growth. The nucleation process occurs when the concentration of the species forming the nanoparticles achieves critical super saturation. Afterwards, three different mechanisms may take place for particle formation [30]:

a) The nucleus formed grows by diffusion of the species inside the solution to the surface of the nucleus until the final size is reached.
b) Nucleation and growth of multiple nuclei occur through the method known as “Ostwald ripening”, in which the smaller nuclei formed are adsorbed into larger nuclei.
c) And finally the particles may be formed more likely by aggregation of small units than by continuous growth due to diffusion.

The occurrence of one type of growth or another depends greatly on the preparation conditions such as temperature, stirring, pH and time, among the most relevant. In the working conditions described here, it seems clear that, when co-precipitation and sonochemistry methods are used, the first of the mentioned mechanisms produces

very small nanoparticles due to maximum nucleation [31,32]. The formation of intermediates in the reaction is, therefore, also due to the high speed of the process and the presence of oxygen during synthesis, giving rise to the formation of iron hydroxides and oxyhydroxides that are unable to react with the dissolved nickel to give ferrite [33]. In the case of E and SE methods, the control over species concentration in the solution is greater and, although they could grow as in the preceding methods (CP and SC), the generation of ions is slower with nuclei growing out of the first ones formed. Once the formed nucleus reaches its critical size, it becomes surrounded by surfactant molecules that inhibit subsequent growth [34].

The lattice parameters for the nickel ferrite phase calculated through the Rietveld refinement for samples E and SE were respectively 0.839 and 0.855 nm. Fig. 1e shows, as an example, the results of the refinement carried out for the electrochemically obtained sample. The value obtained for sample E is similar to that of the unit cell typically assigned to nickel ferrite, with a value of $a=0.833$ nm [28]. In the case of the sample obtained by SE, the lattice parameter is higher than that of the corresponding nickel ferrite, thus indicating that the lattice is distorted, with defects, especially in the case of samples presenting a smaller crystallite size (SE method).

TEM micrographs are shown in Fig. 2. As can be seen in the case of the nanoparticles obtained by CP (Fig. 2a) and SC (Fig. 2b), the particle size is very small and their agglomeration is considerable, so it is very difficult to determine their diameter and distribution. The sheet formation is also visible, due to ferrihydritic compounds. On the other hand, micrographs for the samples obtained by the E and SE methods (Fig. 2c and d) show spherical particles with sizes in the order of 40 and 30 nm, respectively, consistent with the results obtained using X-ray diffraction.

In order to determine the composition and Fe/Ni ratio in these samples, the mass ICP analyses were performed giving values of 3.65, 2.47, 2.08 and 2.18 for samples obtained by CP, SC, E and SE, respectively. As can be seen, only the sample obtained using the E method shows a Fe/Ni ratio close to 2, i.e. a virtually stoichiometric relationship between the two metals; the other samples present iron in excess, confirming that the peaks appearing in the diffractograms should correspond to iron compounds.

It should be mentioned that the CP method is the one presenting the largest number of impurities in the samples obtained. This is one of the main problems presented by this method, since there is no control over the size or composition. For this reason, for obtaining the purest nanoparticles it is necessary to submit the particles to a purification process consisting of filtering the particles and successive rinsing to eliminate the excess of iron hydroxides formed.

The Mössbauer spectra of the samples obtained via CP and SC are shown in Fig. 3(a and b) respectively. In both cases the spectra consist in a quadrupole doublet which, in the case of the sample obtained by CP, presents the following fitting parameters: isomer shift (δ) 0.319(2) mm/s and quadrupole splitting (QS) 0.646(2) mm/s. In the case of the sample obtained using the SC method, the parameters obtained through the fitting are as follows: isomer shift (δ) 0.330(1) mm/s and quadrupole splitting (QS) 0.677(2) mm/s. These parameters are characteristic of high-spin Fe (III) compounds. Therefore, these could be assigned to the nickel ferrite with a size of less than 10 nm with a superparamagnetic behavior or to a paramagnetic oxide/oxyhydroxide, as already confirmed by other techniques.

Fig. 3(c) shows the Mössbauer spectrum at room temperature for electrosynthesized $NiFe_2O_4$. This spectrum is the result of the overlapping of two magnetic sub-spectra with the following hyperfine parameters: isomer shift (δ) 0.315(2) mm/s, quadrupole splitting (QS) 0.02(1) mm/s and hyperfine magnetic field (H) 44.7 T and $\delta=0.552(7)$ mm/s, QS=0.00(1) mm/s and $H=48.4(2)$ T, corresponding to Fe^{3+} located respectively in the tetrahedral and octahedral positions on the spinel. The hyperfine magnetic field values are lower than the expected values of 50.6 T and 54.8 T [35-37] for both positions, being an indicative of the material's nanometric size. The percentage of Fe in tetrahedral position is 57%, slightly higher than the value corresponding to a totally inverse spinel structure. Superimposed to both sextets, it is also

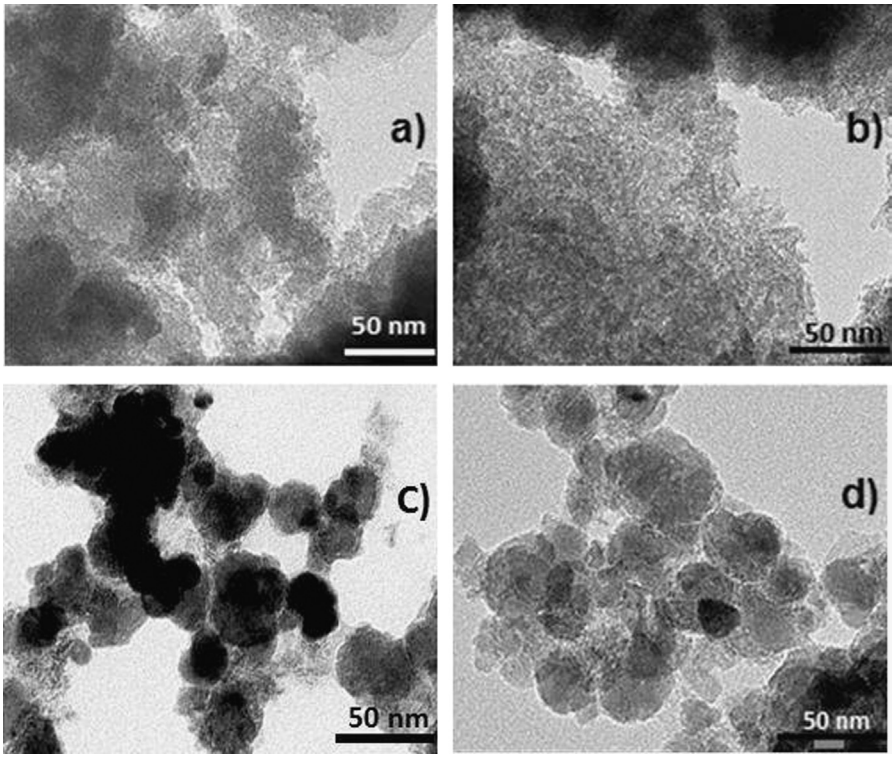

Fig. 2. TEM micrographs of the nanoparticles obtained by (a) coprecipitation, (b) sonochemistry, (c) electrochemistry and (d) sonoelectrochemistry.

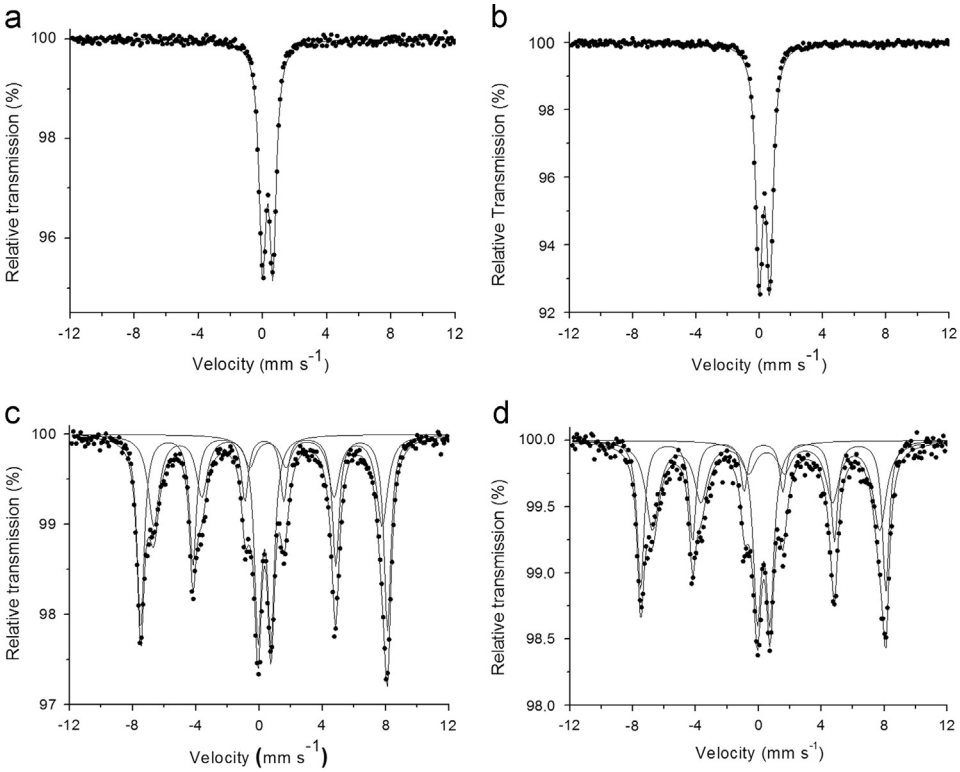

Fig. 3. Mössbauer spectra of the samples obtained via (a) coprecipitation, (b) sonochemistry, (c) electrochemistry and (d) sonoelectrochemistry.

possible to observe the presence of a doublet with parameters $\delta=0.342(3)$ mm/s and QS=0.825(5) mm/s, that could be associated with the presence of 22% of $NiFe_2O_4$ particles with a size close to 10 nm, a size that would explain their superparamagnetic character. Using Mössbauer spectroscopy, it is not possible to rule out the presence of other paramagnetic or superparamagnetic Fe^{3+} oxides, as their spectrum would be similar to that of the doublet [38,39].

The Mössbauer spectrum of the sample obtained by SE (Fig. 3d) is similar to one of the samples obtained electrochemically. It consists of two magnetic sub-spectra with the following hyperfine parameters: isomer shift (δ) 0.312(2) mm/s, quadrupole splitting (QS) 0.02(1) mm/s and hyperfine magnetic field (H) 44.8(1) T and $\delta=0.51(1)$ mm/s, QS=0.04(2) mm/s and $H=48.3(4)$ T, corresponding to the Fe^{3+} respectively located in the tetrahedral and octahedral positions of the spinel. In addition, it is possible to observe the presence of the doublet exhibiting $\delta=0.322(6)$ mm/s and QS=0.81(1) mm/s that, as mentioned previously, would correspond to 23% of $NiFe_2O_4$ particles less than 10 nm in size.

Fig. 4a and 4b show the XPS spectra for the regions of Ni(2p) and Fe(2p) measured for representative samples of nanoparticles of Fe and Ni ferrites synthesized through CP, SC, E and SE, respectively. Two main peaks can be observed at 710.3 eV and 855.5 eV, corresponding to Fe $2p_{3/2}$ and Ni $2p_{3/2}$ energy levels. The position of these peaks corresponds to the bonding energy values referenced in the bibliography for the cations Ni^{2+} [40] and Fe^{3+} [41] for a $NiFe_2O_4$ type iron–nickel oxide. Additionally, different peaks corresponding to the orbitals Fe $2p_{1/2}$ ($\approx$ 724.4 eV) and Ni $2p_{1/2}$ ($\approx$ 873 eV) and the typical satellites of this compound are resolved in the spectra. These results show that in the four methods the surface of the nanoparticles have similar characteristics.

On the TGA and DTA curves measured for the sample obtained by CP, and shown in Fig. 5a, two clear exothermic processes can be distinguished at temperatures of 100 °C and 200 °C. This first weight loss that occurs at 100 °C is associated with the loss of water adsorbed on the sample. After this value, the thermogram shows a gradual reduction in weight, associated with the breakdown of the iron oxyhydroxides [42]. No other peaks are observed at higher temperature values. A similar thermogram is observed for sample obtained through SC (not shown). Fig. 5b shows the TGA and DTA of the sample obtained through E method. In this case the exothermic peak due to desorption of water at approximately 100 °C is also observed. A second peak is observed at 250 °C which should be associated with the breakdown of the organic compound acting as surfactant. Furthermore, a peak is observed at 400 °C that could arise from the phase transition between γ-Fe_2O_3 and α-Fe_2O_3 [28,42]. This behavior could be an indicative of the presence of impurities γ-Fe_2O_3 in these samples, a fact that is in agreement with the slightly higher (2.08) value for the Fe/Ni ratio and the non-distinction with X-rays or Mössbauer since the two compounds present the same spinel structure and similar hyperfine parameters. In the case of the sample obtained via sonoelectrochemistry (TGA not shown), a very broad peak appears around 200 °C, attributed to simultaneous breakdown of the oxyhydroxides and the surfactant [42]. In the same way, there is a peak at 400 °C that may be ascribed to the same process as mentioned above .

Magnetic characterization points out two markedly different magnetic behaviors depending on the synthesis method. Hysteresis loops measured at different temperatures for samples obtained by means of the CP and SC methods are shown in Fig. 6a and b respectively. Almost no differences between both set of samples are observed indicating that the microstructure obtained by both procedures is quite similar in agreement with the observations carried out by TEM. The samples exhibit a ferromagnetic behavior at low temperatures, although it should be noticed that the magnetization is far from saturation, whereas for temperatures above 50 K coercivity and remanence become negligible, see inset of Fig. 6a. The lack of coercivity and remanence is indicative of a superparamagnetic behavior, confirming the results obtained by the Mössbauer spectroscopy. Moreover, the magnetization curves measured at different temperatures superimpose when the magnetization is plotted as a function of H/T. The later behavior is a fingerprint

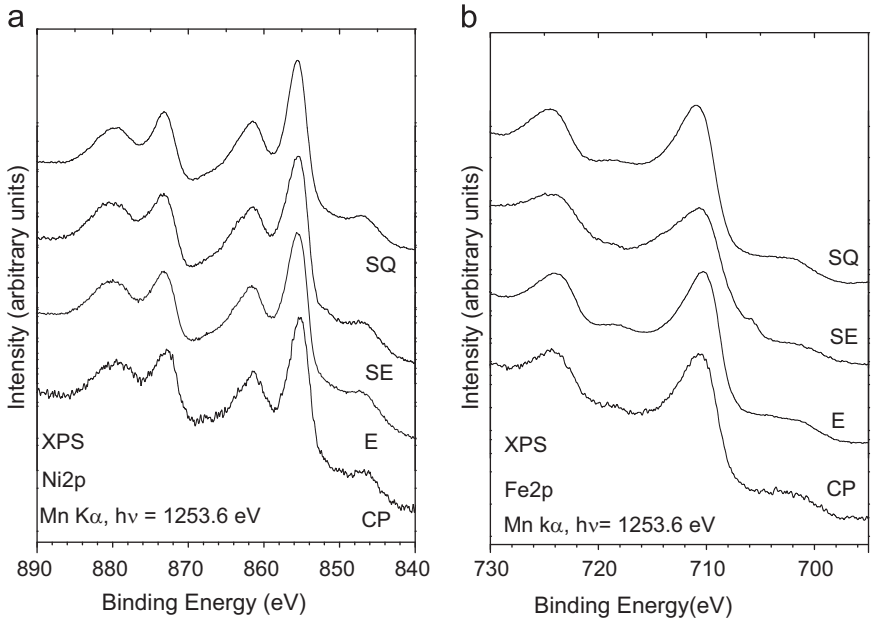

Fig. 4. XPS spectra of nickel ferrite particles synthesized using different synthesis methods (as labeled): (a) Ni 2p region XPS spectra and (b) Fe 2p region XPS spectra.

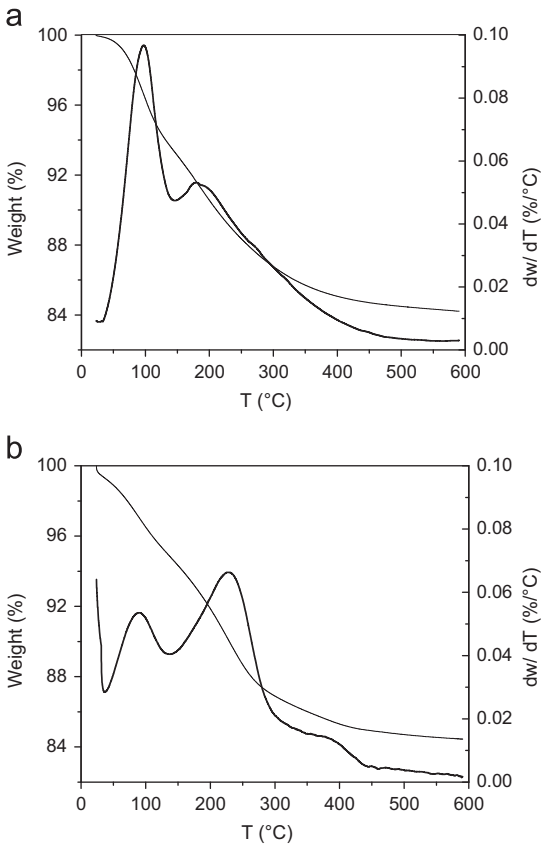

Fig. 5. TGA and DTA for the sample obtained by (a) co-precipitation and (b) electrochemistry, with rates of heating of 50 °C/min from 0.1 to 600 °C in N_2 atmosphere.

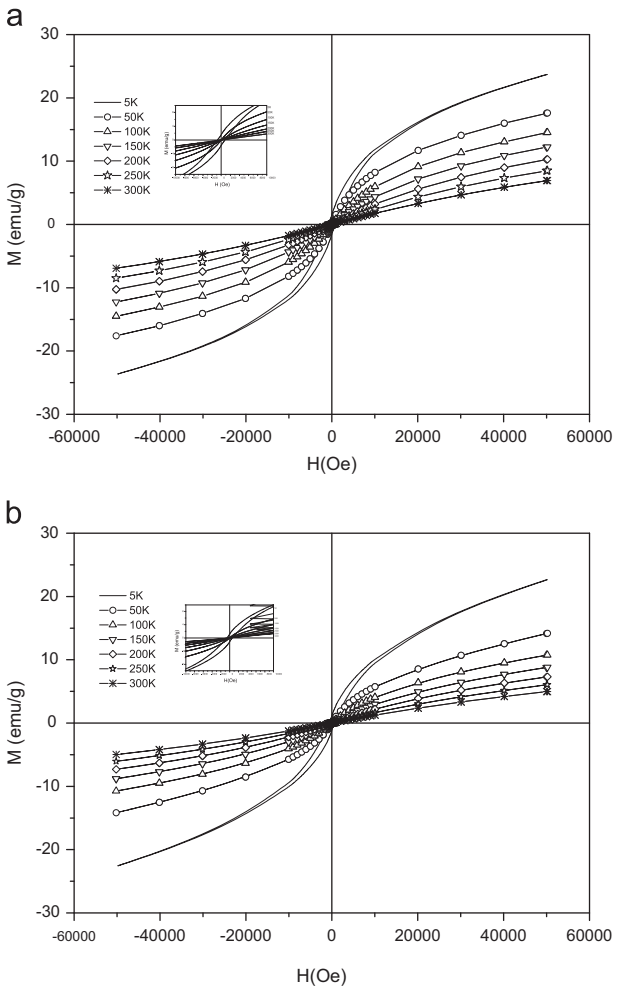

Fig. 6. Magnetization curves at different temperatures of nickel ferrite obtained: (a) coprecipitation and (b) sonochemistry. Inset shows a magnification at low field.

of a system composed by superparamagnetic particles. In both cases, the magnetization at 50,000 Oe is below 30 emu/g which is much lower than that expected for a $NiFe_2O_4$ ferrite, 61 emu/g. This behavior in combination with the superparamagnetic behavior suggests the coexistence of the nickel ferrite phase with other non-magnetic phases. Fig. 7 shows the thermal dependence of the magnetization measured under zero (ZFC) and field cooling (FC) conditions under an applied magnetic field of 1000 Oe for the sample produced by the CP method. A blocking temperature of 25 K can be clearly observed. Similar curves are obtained for the sample

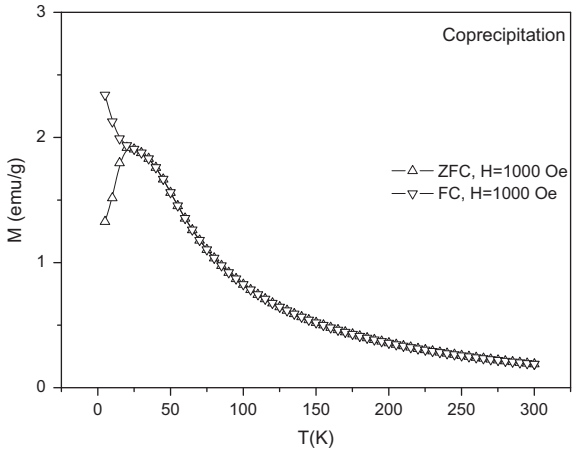

Fig. 7. Thermal dependence of the magnetization measured under zero and field cooling conditions. The system exhibits a blocking temperature of 25 K.

obtained by means of the SC procedure, although in this case the blocking temperature is 30 K.

Assuming that the only magnetic phase is the $NiFe_2O_4$ ferrite that exhibits a cubic structure with an anisotropy constant of $K_1 = -7$ kJ/m^3, an estimation of the average particle size can be obtained through the well known relationship for superparamagnetic systems $kV = 25K_BT$ where k is the anisotropy constant, V is the volume of the nanoparticle, K_B the Boltzmann constant and T the absolute temperature. By considering a blocking temperature of around 30 K the average particle size is estimated to be around 7 nm, in agreement with the results obtained by TEM. It seems that the samples produced via CP and SC procedures are composed by nanoparticles of Ni ferrite with an average particle size of around 7 nm surrounded or embedded in a non-magnetic matrix of ferritic compounds that magnetically isolate the nanoferrite promoting a superparamagnetic behavior. The lack of magnetization saturation could be attributed to the superparamagnetic behavior of the nanoparticles or, additionally, to a spin canting of the magnetic moments located at the nanoparticle surface.

As mentioned, the second set of samples, samples produced by electrochemical-based procedures, exhibit completely different magnetic features. As an example, the magnetization curves measured for the sample obtained by electrochemical route is shown in Fig. 8a whereas Fig. 8b shows the magnetization measured under zero (ZFC) and field cooling (FC) conditions. Similar behavior is observed for the SE synthesized sample. Both measurements indicate that samples are ferromagnetic in the whole temperature measurement range, up to 300 K. This behavior is in clear agreement with the results obtained by TEM studies that showed particles with an average particle size much higher than that of the samples obtained by CP and SQ methods. At low temperatures the samples are not saturated, a behavior that could be related with the presence of some spin-canting at the surface of the particles. The magnetization values at 5 K and at 50,000 Oe are quite similar for both samples and are close to that of the $NiFe_2O_4$ ferrite, 61 emu/g confirming that electrochemical methods allows the synthesis of nearly stoichiometric nickel ferrites. The coercive field decreases with temperature as expected in a ferromagnetic material.

5. Conclusions

This paper clearly shows that the electrochemical method for obtaining nickel ferrite, when compared to other methodologies such as co-precipitation, sonochemistry and sonoelectrochemistry under similar synthesis conditions, temperature, pH and time, and without subsequent treatment, gives rise to nanoparticles very close to stoichiometry, free from intermediate compounds, such as

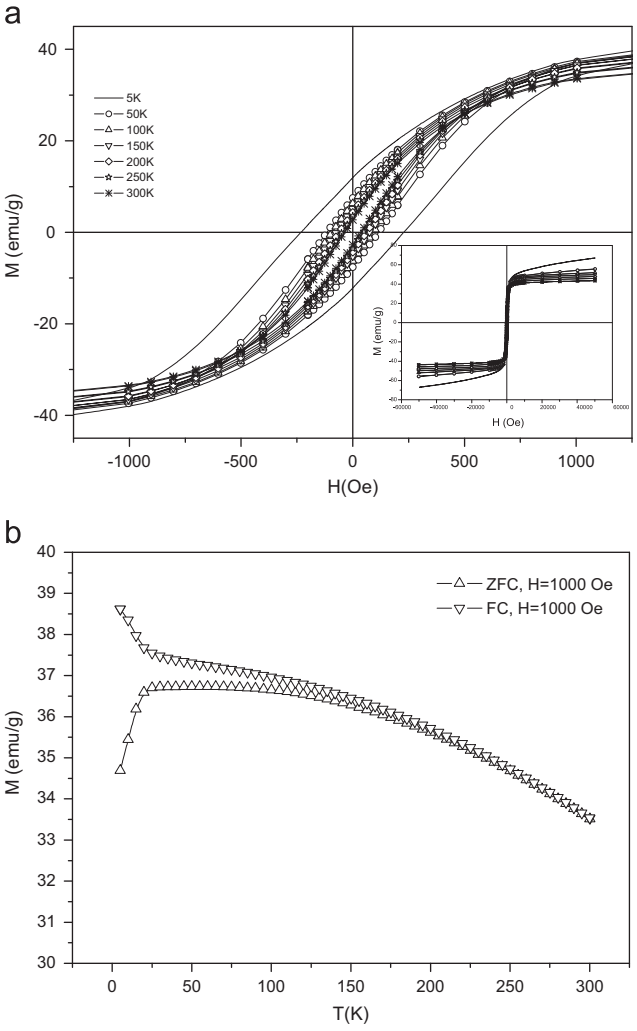

Fig. 8. (a) Magnetization curves at different temperatures of nickel ferrite obtained by electrochemical method. Inset shows complete magnetization curves. (b) Thermal dependence of the magnetization measured under zero and field cooling conditions.

iron or nickel oxyhydroxides, approximately 40 nm in size and with good magnetic characteristics.

The nanoparticles obtained by the co-precipitation and sonochemistry methods show similar characteristics with small sizes and a large number of intermediate compounds in the synthesis reaction, especially iron hydroxides and oxyhydroxides.

As for sonoelectrochemistry, the nickel ferrite nanoparticles present structural and magnetic characteristics similar to those obtained electrochemically, with a smaller size but also with the appearance of some intermediate compounds.

Acknowledgment

This investigation has been funded by the Spanish Ministry of Economy and Competitiveness (MINECO) through MAT2012-37109-C02-01, MAT2012-37109-C02-02 and the CONSOLIDER CSD-00023 and ENE2010-21198-C04-04 Project. OBM thanks the financial support from the "Ramón y Cajal Program" of the MINECO.

References

[1] J.R. McCarthy, R. Weissleder., Adv. Drug Deliv. Rev. 60 (2008) 1241–1251.
[2] D. Huska, J. Hubalek, V. Adam, D. Vajtr, A. Horna, L. Trnkova, L. Havel, R. Kizek., Talanta 79 (2009) 402–411.

[3] J. Esquivel, I.A. Facundo, M.E. Treviño, R.G. López., J. Mater. Sci. 42 (2007) 9015–9020.
[4] Q.A. Pankhurts, J. Connolly, S.K. Jones, J. Dobson., J. Phys. D: Appl. Phys. 36 (2003) R167–R181.
[5] G.F. Goya, V. Grazú, M.R. Ibarra, Curr. Nanosci. 4 (2008) 1–16.
[6] R. Asmatulu, M.A. Zalich, R.O. Claus, J.S. Riffle, J. Magn. Magn. Mater. 292 (2005) 108–119.
[7] Y.S. Kang, S. Risbud, J.F. Rabolt, P. Stroeve, Chem. Mater. 8 (9) (1996) 2209–2211.
[8] S.H. Sun, H. Zeng, J. Am. Chem. Soc. 124 (28) (2002) 8204–8205.
[9] R.J. Rennard, W.L. Kehl., J. Catal. 21 (1971) 282–286.
[10] N. Tsubokawa, T. Kimoto, T. Endo., J. Mol., A Catal., Chemical 101 (1995) 45–49.
[11] E. Manova, T. Tsoncheva, D. Paneva, J.L. Rehspringer., K. Tenchev, L. Mitov, L. Petrov., Appl. Catal. A: Gen 317 (2007) 34–38.
[12] S.P. Ghorpade, V.S. Darshane, S.G. Dixit., Appl. Catal. A 166 (1998) 135–141.
[13] Y. Mu, D. Jia, Y. He, Y. Miao, H. Wu., Biosens. Bioelectron. 26 (2011) 2948–2952.
[14] R. Ramanathan, S. Sugunan., Catal. Commun. 8 (2007) 1521–1526.
[15] C.G. Ramankutty, S. Sugunan, Appl. Catal. A: Gen. 218 (2001) 39–51.
[16] S. Singh, K.C. Barick, D. Bahadur., J. Hazard. Mater. 192 (2011) 1539–1547.
[17] J.F. Liu, Z-S. Zhao, G.B. Jiang, Environ. Sci. Technol. 42 (2008) 6949–6954.
[18] Y.F. Shen, J. Tang, Z.H. Nie, Y.D Wang, Y. Ren, L. Zuo., Sep. Purif. Technol. 68 (2009) 312–319.
[19] Li-H. Liu, H. Dietsch, P. Schurtenberger, M. Yan, Bioconjugate Chem. 20 (2009) 1349–1355.
[20] A.E. Berkowitz, R.H. Kodama, S.A. Makhlouf, F.T. Parker, F.E. Spada, E.J. McNiff , S. Foner., J. Magn. Magn. Mater. 196–197 (1999) 591–594.
[21] J. Zhang, J. Shi, M. Gong., J. Solid State Chem. 182 (2009) 2135–2140.
[22] Y. Cheng, Y. Zheng, Y. Wang, F. Bao, Y. Qin., J. Solid State Chem. 178 (2005) 2394–2397.
[23] S. Maensiri, C. Masingboon, B. Boonchomb, S. Seraphin., Scr. Mater. 56 (2007) 797–800.
[24] S.A.S. Ebrahimi, J. Azadmanjiri., J. Non-Cryst. Solids 353 (2007) 802–804.
[25] M.M. Rashad, O.A. Fouad., Mater. Chem. Phys. 94 (2005) 365–370.
[26] A.S. Albuquerque, J.D. Ardisson, W.A.A. Macedo, J.L. López, R. Paniago, A.I.C. Persiano., J. Magn. Magn. Mater. 226–230 (2001) 1379–1381.
[27] R.A. Brand, Nucl. Instrum. Methods Phys. Res. B 28 (1987) 398.
[28] S. Maensiri, C. Masingboon, B. Boonchomb, S. Seraphin., Scr. Mater. 56 (2007) 797–800.
[29] B.D. Cullity, S.R. Stock, Elements of X-ray Diffraction, third ed., Prentice-Hall, Englewood Cliffs, NJ, 2001.
[30] P. Tartaj, M.P. Morales, S. Veintemillas-Verdaguer, T González-Carreño, C.J. Serna., J. Phys D: Appl. Phys. 36 (2003) R182.
[31] J. Zhang, J. Shi, M. Gong., J. Solid State Chem. 182 (2009) 2135–2140.
[32] C.G. Ramankutty, S. Sugunan., Appl. Catal. A: Gen. 218 (2001) 39–51.
[33] N.S. McIntyre, D.G. Zetaruk., Anal. Chem. 49 (1977) 1521–1526.
[34] A. Aqil, H. Serwas, J.L. Delplancke, R. Jérôme, C. Jérôme, L. Canet., Ultrason. Sonochem. 15 (2008) 1055–1061.
[35] E. Manova, T. Tsoncheva, D. Paneva, J.L. Rehspringer, K. Tenchev, I. Mitov, L. Petrov., App. Catal. A: Gen. 317 (2007) 34–42.
[36] N.N. Greenwod, T.C. Gibb, Mössbauer Spectroscopy, Chapman and Hall Ltd, 1971.
[37] R.N. Panda, N.S. Gajbhiye, G. Balaji., J. Alloys Compd. 326 (2001) 50–53.
[38] S. Morup, J. Magn. Magn. Mater. 37 (1983) 39–50.
[39] S. Morup, H. Topsoe., J. Magn. Magn. Mater. 31–34 (1983) 953–954.
[40] K.K. Lian, D.W. Kirk, S.J. Thorpe., J. Electrochem. Soc. 142 (1995) 3704–3709.
[41] J. Zhang, J. Shi, M. Gong., J. Solid State Chem. 182 (2009) 2135–2140.
[42] C.G. Ramankutty, S. Sugunan., Appl. Catal. A: Gen. 218 (2001) 39–51.